ARL-TR-9166 ● APR 2021

DEVCOM ARMY RESEARCH LABORATORY

Agile Expedient Manufacturing (Summary Technical Report, 2018–2020)

by Marc Pepi, Brandon McWilliams, and Andelle Kudzal

NOTICES

Disclaimers

The findings in this report are not to be construed as an official Department of the Army position unless so designated by other authorized documents.

Citation of manufacturer's or trade names does not constitute an official endorsement or approval of the use thereof.

Destroy this report when it is no longer needed. Do not return it to the originator.

ARL-TR-9166 ● APR 2021

Agile Expedient Manufacturing (Summary Technical Report, 2018–2020)

Marc Pepi, Brandon McWilliams, and Andelle Kudzal
Weapons and Materials Research Directorate,
DEVCOM Army Research Laboratory

REPORT DOCUMENTATION PAGE

Form Approved
OMB No. 0704-0188

1. REPORT DATE *(DD-MM-YYYY)*	2. REPORT TYPE	3. DATES COVERED (From - To)
April 2021	Summary Technical Report	1 October 2018–30 September 2020

4. TITLE AND SUBTITLE
Agile Expedient Manufacturing (Summary Technical Report, 2018–2020)

5a. CONTRACT NUMBER

5b. GRANT NUMBER

5c. PROGRAM ELEMENT NUMBER

6. AUTHOR(S)
Marc Pepi, Brandon McWilliams, and Andelle Kudzal

5d. PROJECT NUMBER

5e. TASK NUMBER

5f. WORK UNIT NUMBER

7. PERFORMING ORGANIZATION NAME(S) AND ADDRESS(ES)
DEVCOM Army Research Laboratory
ATTN: FCDD-RLW-MD
Aberdeen Proving Ground, MD 21005-5069

8. PERFORMING ORGANIZATION REPORT NUMBER
ARL-TR-9166

9. SPONSORING/MONITORING AGENCY NAME(S) AND ADDRESS(ES)

10. SPONSOR/MONITOR'S ACRONYM(S)

11. SPONSOR/MONITOR'S REPORT NUMBER(S)

12. DISTRIBUTION/AVAILABILITY STATEMENT
Approved for public release: distribution unlimited.

13. SUPPLEMENTARY NOTES
ORCID ID: Marc Pepi, 0000-0003-0691-5925; Brandon McWilliams, 0000-0002-0494-3140

14. ABSTRACT
The capability of metal additive manufacturing (AM) on the future battlefield holds many promises, as well as numerous challenges. This technology would most likely provide the warfighter with an agile means of repairing battle damage as well as the ability to manufacture spare parts at the point of need, thereby reducing reliance on the traditional supply chain while improving operational readiness. An important cog in this vision would be the capability to produce AM-grade metallic powder in-theater from recycled and reclaimed battlefield scrap to further reduce the military logistics tail. This technical report summarizes the work encompassing the production of AM-grade metallic powder from scrap and the results of subjecting these powders to subsequent AM operations toward agile expedient manufacturing, and ultimately, transformational overmatch.

15. SUBJECT TERMS
STR, 3-D printing, additive manufacturing, AM, point-of-need manufacturing, mechanical testing, operational readiness

16. SECURITY CLASSIFICATION OF:			17. LIMITATION OF ABSTRACT	18. NUMBER OF PAGES	19a. NAME OF RESPONSIBLE PERSON
a. REPORT	b. ABSTRACT	c. THIS PAGE			Marc Pepi
Unclassified	Unclassified	Unclassified	UU	53	19b. TELEPHONE NUMBER (Include area code) 410-306-0848

Contents

List of Figures

List of Tables

Acknowledgments

The authors thank Danielle Cote, Bryer Sousa, Derek Tsaknopoulos, Chris Massar, Kyle Fitzpatrick-Schmidt, Caitlin Walde, Matt Gleason, and Jack Grubbs (Worcester Polytechnic Institute) as well as Luvak Laboratories for powder characterization; Clara Mock and Josh Taggart-Scarff (US Army Combat Capabilities Development Command Army Research Laboratory) for metallography and microhardness support; Jian Yu for ballistic testing and analysis; Kevin Doherty (ARL) for MELD Manufacturing research and development information, as well as Chase Cox and Nanci Hardwick of MELD Manufacturing for their support with additive friction stir processing; Sharon Park and Yongho Sohn from the University of Central Florida for powder characterization; Mark Graybeal, The Johns Hopkins University–Applied Physics Laboratory (ARL) for cold-spray support; Jennifer Sietins and Jessica Sun (ARL) for computed tomography support; Joey Griffiths, and Hang Yu of Virginia Tech for metallography and electron-backscatter-diffraction support; and Chris Eonta, Andrew LaTour, and Matthew Charles from MolyWorks Materials Corporation for providing the powders for this study.

Executive Summary

This work focused on the capability of producing gas-atomized AM-grade metallic powder at the point of need from battlefield scrap, and subsequent AM operations as a proof-of-concept that these powders would be useful and viable for component repair and replacement to enhance future Army operational readiness. The authors believe this capability could provide the Army with agile expedient manufacturing capabilities in austere environments and, ultimately, transformational overmatch.

The capability of metal additive manufacturing (AM) on the future battlefield holds many promises, and numerous challenges. This technology would most likely provide the warfighter with an agile means of repairing battle damage as well as the ability to manufacture spare parts at the point of need, thereby reducing reliance on the traditional supply chain while improving operational readiness. An important cog in this vision would be the capability to produce AM-grade metallic powder in-theater from recycled and reclaimed battlefield scrap to further reduce the military logistics tail. This technical report summarizes the work encompassing the production of AM-grade metallic powder from scrap and the results of subjecting these powders to subsequent AM operations toward agile expedient manufacturing and, ultimately, transformational overmatch.

1. Introduction

This report summarizes the work performed under the Agile Expedient Manufacturing mission program during FY19–FY20. The primary deliverable for this research was to demonstrate feasibility of metal additive manufacturing (AM) using material feedstock derived from "indigenous sources". In this case, indigenous sources was actual aluminum (Al) battlefield scrap provided by the National Ground Intelligence Center (NGIC) at Aberdeen Proving Ground (APG), Maryland, and rolled homogeneous armor (RHA) found on Spesutie Island, APG, both intended to simulate materiel that would potentially be available at the point of need. US Army Directive 2019-29, *Enabling Readiness and Modernization through Advanced Manufacturing*, envisions advanced manufacturing transforming battlefield logistics through on-demand fabrication of parts close to the point of need.[1] Toward this end goal, the US Army Combat Capabilities Development Command Army Research Laboratory is researching technologies that will make it possible for the warfighter to manufacture and/or repair components at the point of need with scrap materials on-hand, thus increasing operational readiness while reducing the military logistics footprint. The objective of this project was to show a proof-of-concept of additively manufacturing with metal powder gas-atomized from the aforementioned scrap in a mobile foundry housed within a shipping container. The resultant Al powder was subjected to cold-spray repair as well as additive friction stir processing (AFSP), while the RHA powder was subjected to laser powder bed fusion (LPBF), for builds that were tested metallurgically and ballistically. The cursory results listed herein showed that the AM builds from powder made from scrap materials can be successfully used for cold-spray and additive friction stir (AFS) repair, as well as LPBF AM builds.

2. Background

One of the many problems encountered with overseas warfare is the logistics involved with transporting materiel to the point of need. In the context of this report, this includes replenishing weapon system repair and/or replacement parts. Although Army units currently carry some parts on hand, it is impossible to know exactly which part is going to fail and surprises will surely be encountered. In some cases, a part failure may render the weapon system idled until the failed part can be replaced or repaired. More times than not, parts can have a long lead time and might not arrive for months. In a worst-case scenario, manufacturers may no longer exist for parts of our aging legacy systems. This is the scenario where point-of-need manufacturing would make a lot of sense as a means to augment our current supply

chain (not replace it) in order to get our systems up and running until the "real" part arrives. The vision set forth in this research is the ability to gas-atomize metal powder from recycled scrap in an ISO (International Organization for Standardization) container for subsequent AM. This would align with the Army's number one priority: "Army readiness". R&D is well underway toward production of metal powder in an ISO container, but metal AM at the point of need is still a ways off as of this writing.

3. Objective/Motivation

As stated in Ransom's *Logistics Transformation – Reducing the Logistics Footprint*, "Technology will be one of the primary enablers to reduce the logistic footprint, and the reduction of the logistic footprint is clearly a key element of the future battlefield".[2] Further, da Silva and Rezende note "The implications of additive manufacturing for logistics could be massive, both for the upstream supply chain and for downstream customer".[3] In addition, Manners-Bell and Lyon have surmised that AM will have implications on logistics by allowing for "near-source" production.[4] To address the role of AM on operational readiness, US Army Directive 2019-29, *Enabling Readiness and Modernization through Advanced Manufacturing*, was published in September 2019. The objectives of this directive include "on-demand fabrication of parts close to the point of need, and the use of advanced manufacturing at the tactical level to reduce the logistics footprint".

According to Dellarocco, "shrinking the logistics tail is an important benefit of utilizing indigenous materials in-theater".[5] To this end, the vision of the research performed herein is to use scrap materiel on the battlefield as feedstock for gas-atomization in an ISO container to enable tactical manufacturing at the point of need with locally harvested and indigenous materials. This report describes efforts conducted within the framework of Task 622144.BL1.02, entitled "Agile Expedient Manufacturing" and performed primarily within the DEVCOM Army Research Laboratory's Weapons and Materials Research Directorate, under the leadership of the listed authors, and summarizes the cursory results of this undertaking from a laboratory setting.

4. MolyWorks Materials Corporation Mobile Foundry

A few technologies have been able to successfully AM using waste materials (or produce AM-grade powder from scrap) with varying potential to operate in an expeditionary setting. Samarjy and Kaplan studied laser cutting as a source of molten droplets for AM and were able to demonstrate a continuous track of waste steel on a steel substrate.[6] Fullenwider et al. used a two-stage ball mill to create

AM-grade powder from recycled machining chips.[7] The processed powder was reportedly near-spherical, exhibited a particle size range of 38–150 μm, and was successfully deposited using laser-engineered net shape (LENS) deposition. Likewise, the MELD AFS process and cold-gas-dynamic-spray technologies have also shown proof-of-concept of being able to deposit powder made from recycled materials.[8] The MELD AFS process has also been used to deposit material from Al machining waste chips.[9] Mahmood et al. have reported AM (through laser direct metal deposition) using carbon-steel machining chips that were waste from a CNC process.[10] Similarly, Jackson et al. used the same AM technology to build with 316L stainless steel machining chips.[11] All of these examples show that this concept is of interest across many diverse disciplines.

In light of the vulnerabilities presented by convoys restocking outposts with vital supplies, it was determined that the capability of gas-atomizing scrap metal in an ISO container to produce AM-grade metal powder at the point of need was a better option than having metal powder shipped via traditional logistics supply channels. This would meet one of the challenges facing metal AM at the point of need. The primary author of this report submitted Small Business Innovative Research (SBIR) topic A16-023, entitled "Processing of Metallic Scrap Materials for Battlefield Additive Manufacturing" in 2017, which was accepted, and ARL awarded MolyWorks Materials Corporation SBIR funding (W911QX-17-C-0025) to research and develop a means to accomplish this. Currently in the Phase II Enhancement stage, Molyworks' Mobile Foundry has produced many different AM-grade metal powders from scrap, including Al, steels, stainless steels, OFE-101 copper (from machining chips), titanium, and more. A photo of the Mobile Foundry contained within an ISO container is shown in Fig. 1. SBIR funding has allowed for increased yields, throughput, and gas efficiency. The technology readiness level of this unit is currently 6 and will be 7 by the end of the Phase II Enhancement.

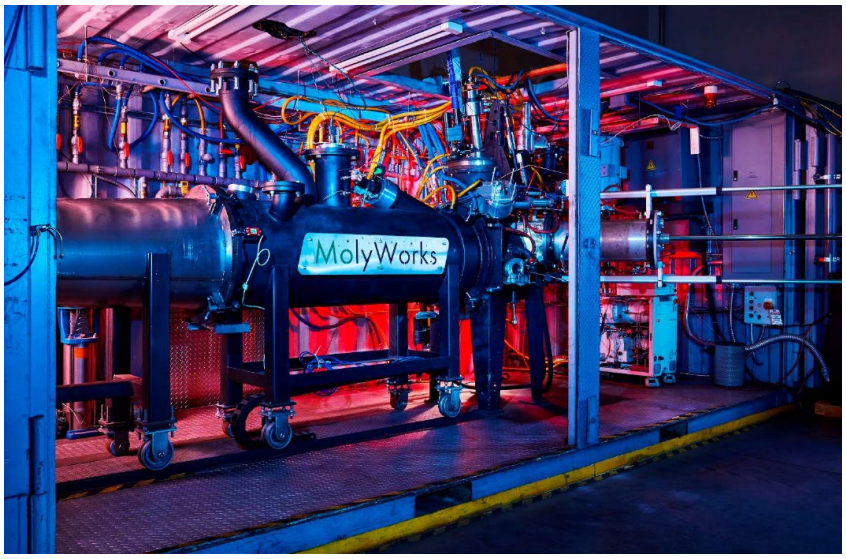

Fig. 1 MolyWorks Materials Corporation Mobile Foundry

Figure 2 depicts the process used within the Mobile Foundry for powder production.

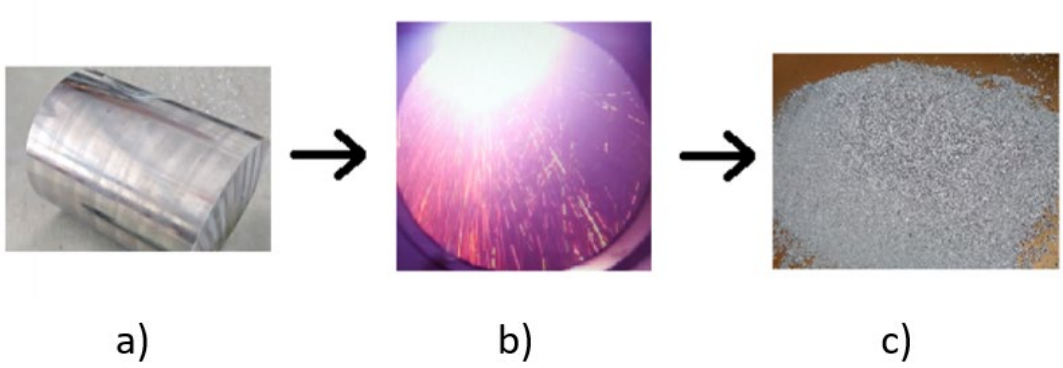

Fig. 2 a) Bulk metal is b) melted within the Mobile Foundry, resulting in c) AM-grade metal powder

5. Metal Recycling

It is well known that recycling provides material savings because of a reduction in the need for mined raw materials, and for most metals, recycling can be performed infinitely in principle.[12] In the commercial sector, the steel circular economy is very well developed (up to 90% recycling rate),[13–17] providing confidence that successful steel recycling could also be performed at the point of need for the military. Scrap materiel would most likely be prevalent at a forward operating base, or contingency operating base close to the point of need. A potential challenge, however, is associated with contamination of the recycled materials (and a resultant reduction in mechanical properties), as residual elements become more abundant

with subsequent recycling.[12,14,17–19] For this reason, the chemical composition of the recycled material will need to be monitored and controlled.

6. Scrap Materials Used

As mentioned, Al scrap from the NGIC and scrap RHA were used as feedstock in the Mobile Foundry for producing AM-grade metallic powders. The Al scrap sent to MolyWorks Corp is shown in Fig. 3. It consisted of a variety of aluminums of different chemistries (as determined by energy dispersive spectroscopy [EDS]) and manufacturing operations. Scrap RHA (Figs. 4a and 4b) was also sent from ARL to MolyWorks for melting and gas-atomization processing within the Mobile Foundry. RHA is used extensively for ballistic resistance[20] and is the principal material employed for military heavy combat and recovery vehicles.[21]

Fig. 3 Scrap Al components melted and turned into AM-grade metal powder in the MolyWorks Mobile Foundry

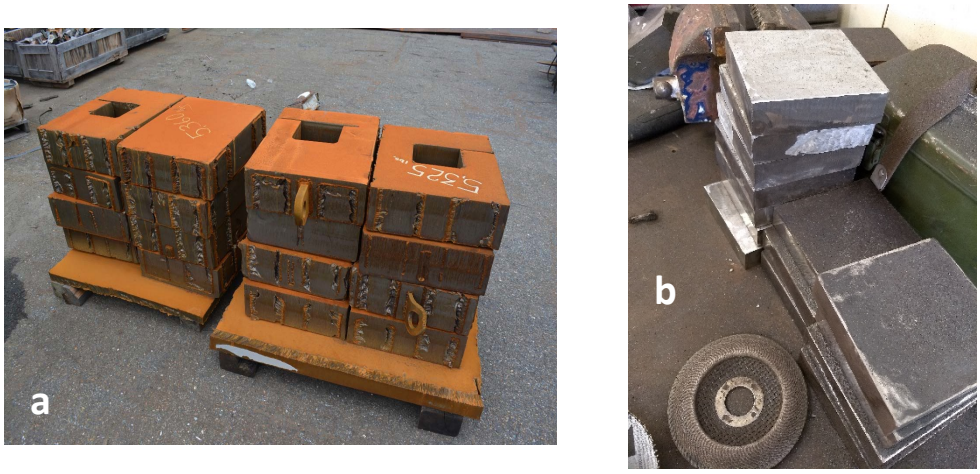

Fig. 4 Two batches of scrap RHA shipped to MolyWorks for melting and gas atomization a) before and b) after grit-blasting to remove corrosion products prior to melting and atomization

After grit-blasting to remove prior coatings, rust, and the like, the material was melted and atomized to AM-grade powder. For the scrap Al, only up to 45 μm was requested and supplied. For the RHA, particle size ranges of 0–45 μm and 45–150 μm were produced and provided to ARL. The 0- to 45-μm particle size distribution is useful for LPBF, cold spray, AFSP, and other AM processes, while the 45- to 150-μm distribution is typical of the range required for LENS deposition. The following sections summarize the results of characterization performed on the resultant powders.

7. Powder Characterization

The Al and RHA powders were subjected to characterization in the form of nanoindentation hardness, metallography, particle size distribution, scanning electron microscopy (SEM), and chemical analysis.

7.1 Nanoindentation Hardness Testing

Nanohardness testing was performed on the powders from scrap by Worcester Polytechnic Institute (WPI). The results shown in Fig. 5.[22] The equipment used was the Keysight G200 Nanoindentation Testing System equipped with a Berkovich diamond indenter tip machined by Micro Star Technologies. The powder from Al scrap showed tight results, with all results falling within the bubble shown. The bubble diagram of elastic modulus versus hardness for the RHA powder had the most error of any of the powders analyzed. RHA "revert" refers to powder made from RHA scrap that was not classified during the initial run in the Mobile Foundry

and subjected to remelt and reprocessing. It was interesting that the hardness of the 0- to 45-μm batches of RHA exhibited higher hardness than the revert batches.

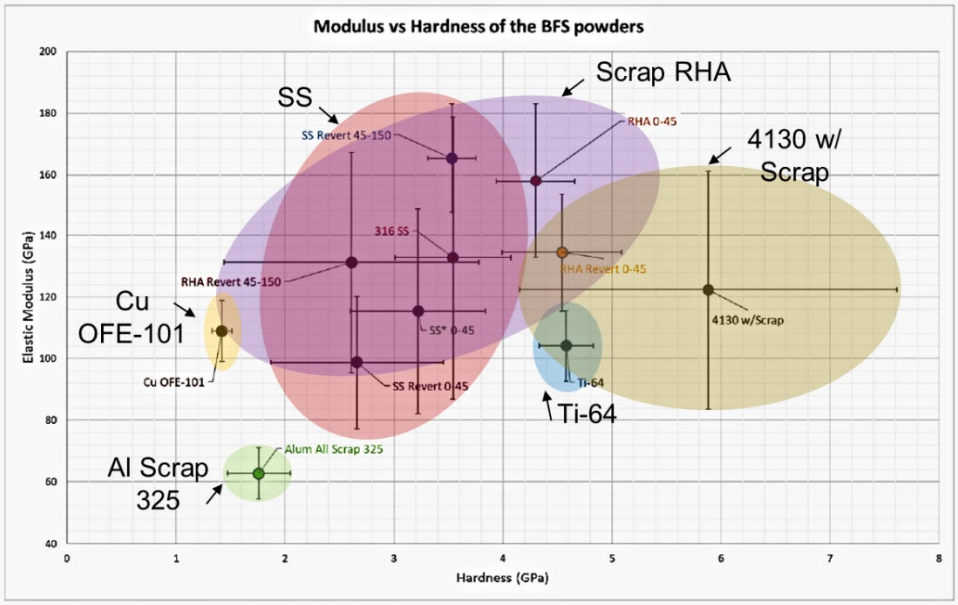

Fig. 5 Results of elastic modulus vs. hardness (as determined through nanoindentation testing) for various powders produced by MolyWorks. Scrap Al bubble plot is colored light green, while the RHA bubble plot is colored purple. Legend: SS = stainless steel, RHA = rolled homogeneous armor, 4130 = AISI 4130 steel, OFE-101 = copper alloy, 325 = –325 mesh size.

7.2 Metallography

Optical microscopy was used to characterize the powders made from scrap. The as-received powder was compression-mounted using a Beuhler Simplimet 4000 mounting system in phenolic resin known as red PhenoCure and polished in a multistage process to produce a mirror finish without compromising the powders' integrity. The mirror finish was obtained using a 0.05-μm colloidal silica suspension and cleaned using ultrasonic vibration in ethanol. The polished samples were subsequently examined using the Olympus GX53 inverted optical microscope. The Al powder is shown in Fig. 6, and the RHA powder is shown in Figs. 7 and 8 for the 0.45-μm and 45- to 150-μm sizes, respectively. Some nonspherical particles were noted in these photomicrographs, which may not be optimal for subsequent AM processes.

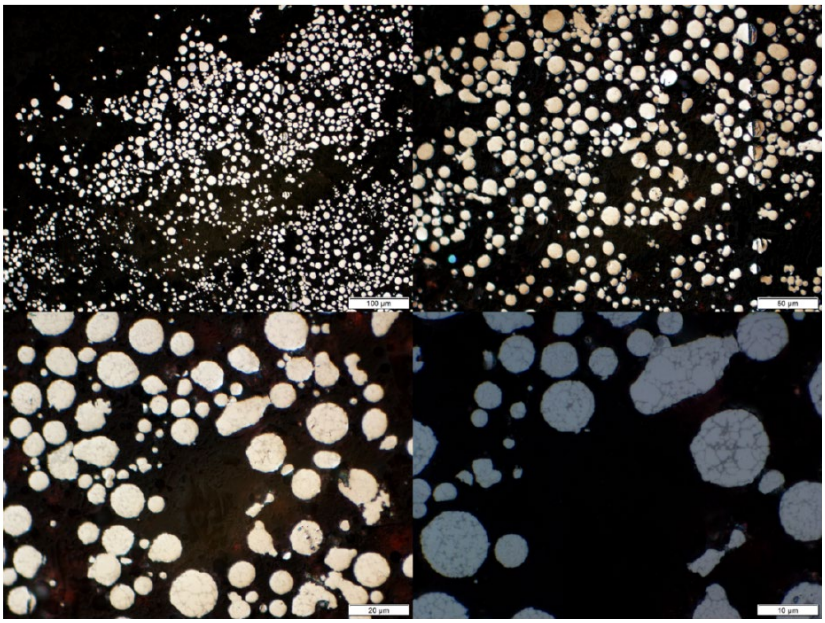

Fig. 6 Optical cross sections of the all-scrap Al powder (–325 mesh) made in the MolyWorks Mobile Foundry at increasing magnifications. Scale bars clockwise from top left are 100, 50, 20, and 10 µm.

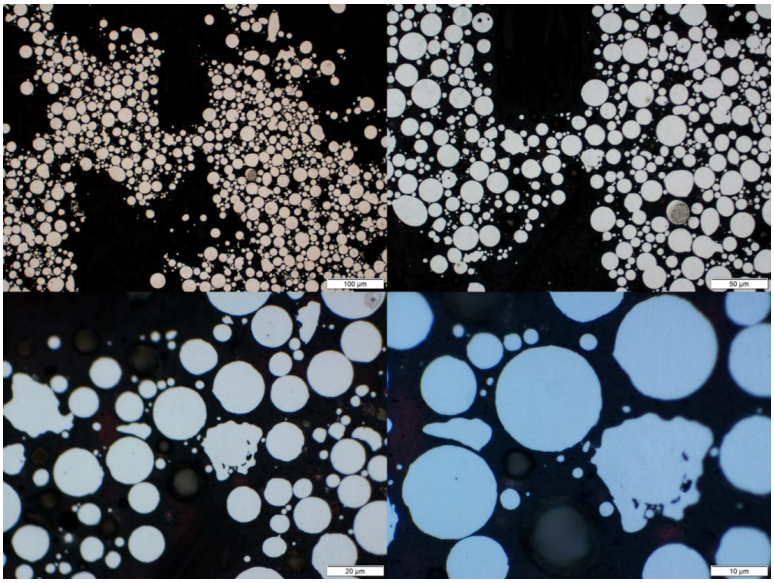

Fig. 7 Optical cross sections of the 0- to 45-µm RHA powder at increasing magnifications. Scale bars clockwise from top left are 100, 50, 20, and 10 µm.

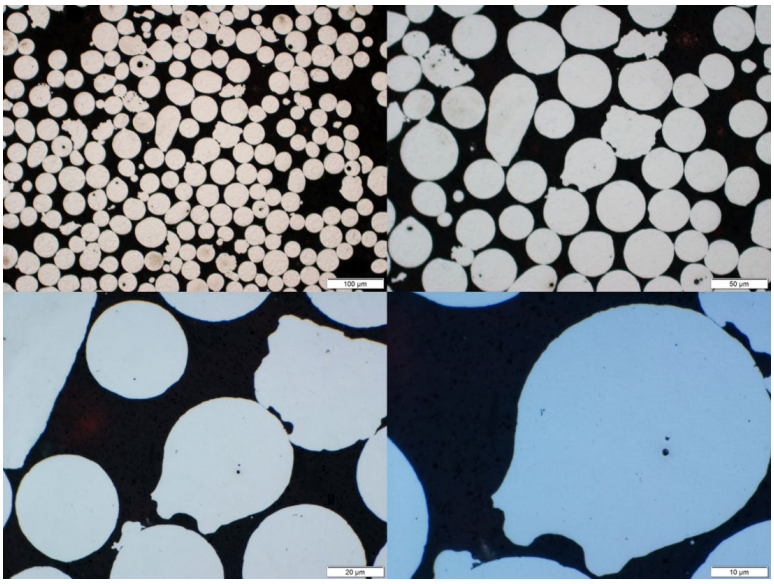

Fig. 8 Optical cross sections of the 45- to 150-µm RHA powder at increasing magnifications. Scale bars clockwise from top left are 100, 50, 20, and 10 µm.

7.3 Particle Size Distribution

The particle size distribution of the powders from scrap was calculated by the University of Central Florida using the Beckman Coulter LS 13 320 using 7 g of the material. The results are displayed in Fig. 9 for the Al powder and in Fig. 10 for the RHA powder. Each of the results showed that the particle size matched the respective designations for this powder.

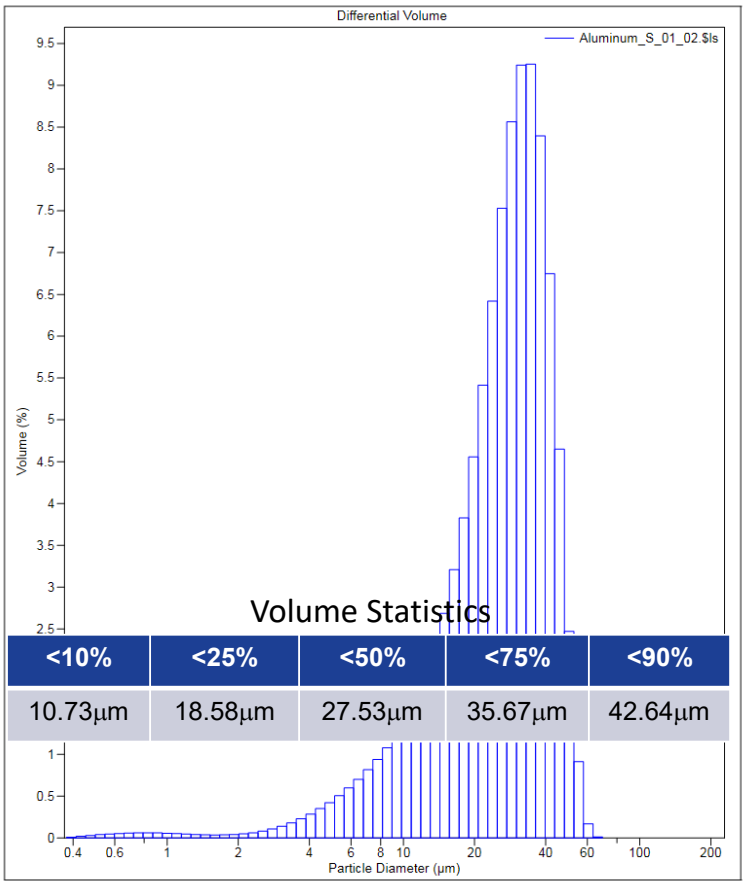

Fig. 9 Particle size distributions of the scrap Al powder. The particle size conformed to the powder designation.

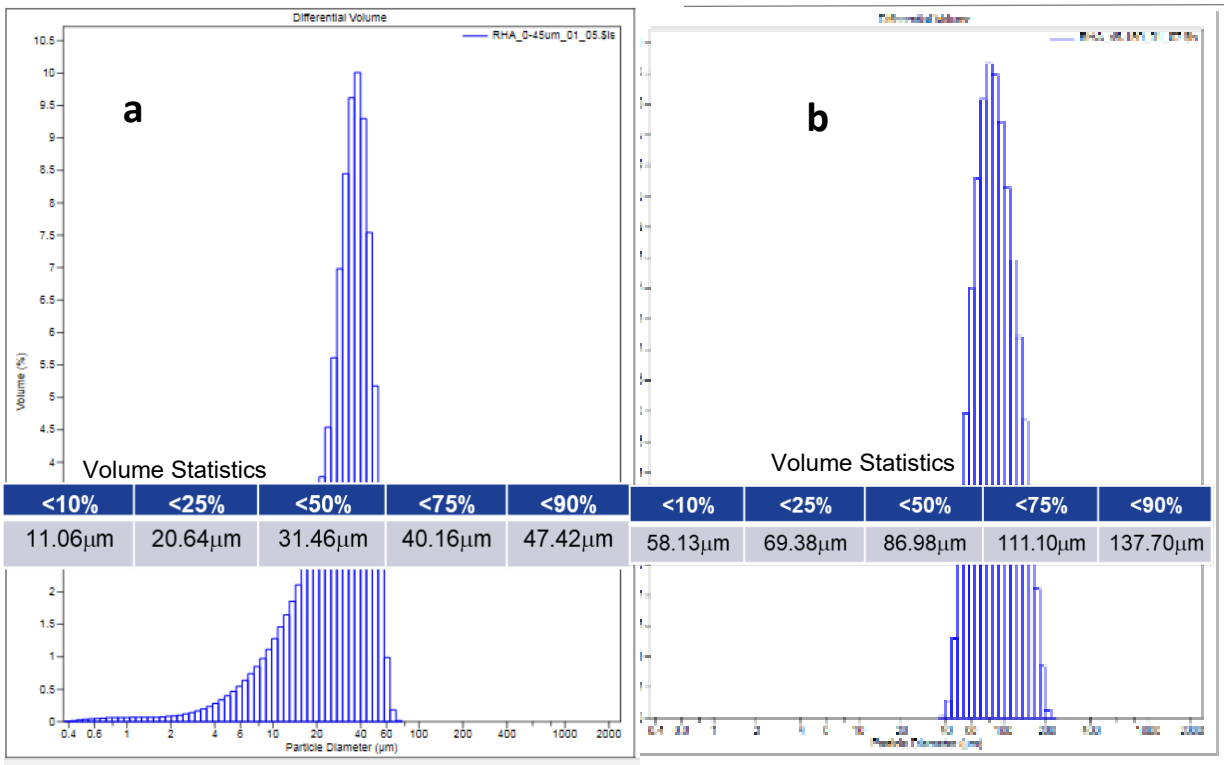

Fig. 10 Particle size distributions of the RHA a) 0- to 45-µm powder and b) 45- to 150-µm powder. Particle size conformed to the powder designations.

7.4 Scanning Electron Microscopy

The SEM used by WPI for this study was a Zeiss Evo Series. The particles were loosely sprinkled upon double-sided SEM mounting tape. To determine homogeneity in terms of geometric particle distribution, SEM imaging was conducted by mounting "loose" powder to a double-sided carbon adhesive stub. To increase imaging quality, the specimens were sputter-coated with gold and palladium particulates. SEM images of powder made from scrap Al are shown in Fig. 11, while images of the 0- to 45-µm and 45- to 150-µm RHA powders are shown in Figs. 12 and 13, respectively. Similar to the optical micrographs presented earlier, many nonspherical particles were noted. Some satellites were also noted, a by-product of the gas-atomization process.

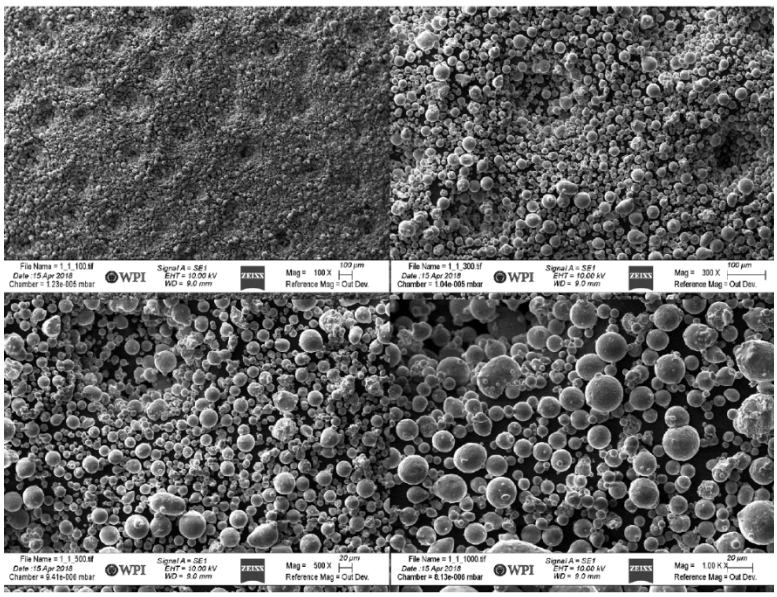

Fig. 11 SEM images of the 0- to 45-µm Al powder. Scale bars clockwise from top left are 100, 100, 20, and 20 µm.

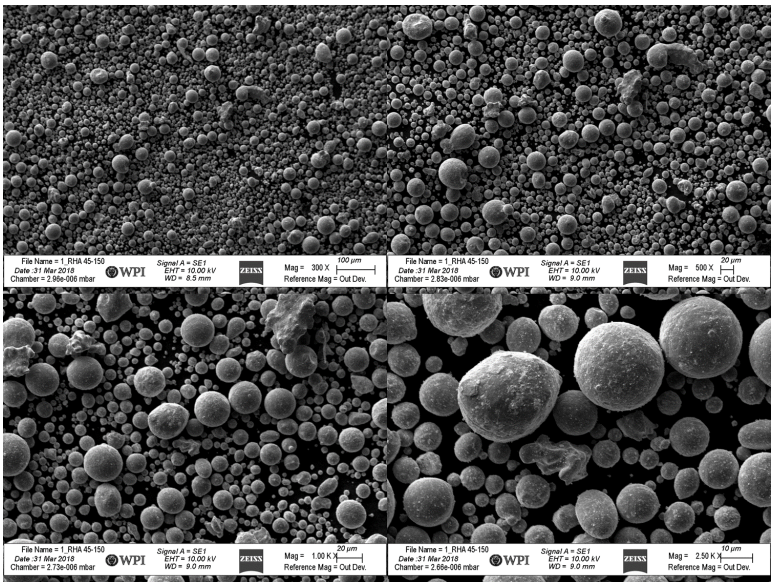

Fig. 12 SEM images of the 0- to 45-µm RHA powder. Scale bars clockwise from top left are 100, 20, 20, and 10 µm.

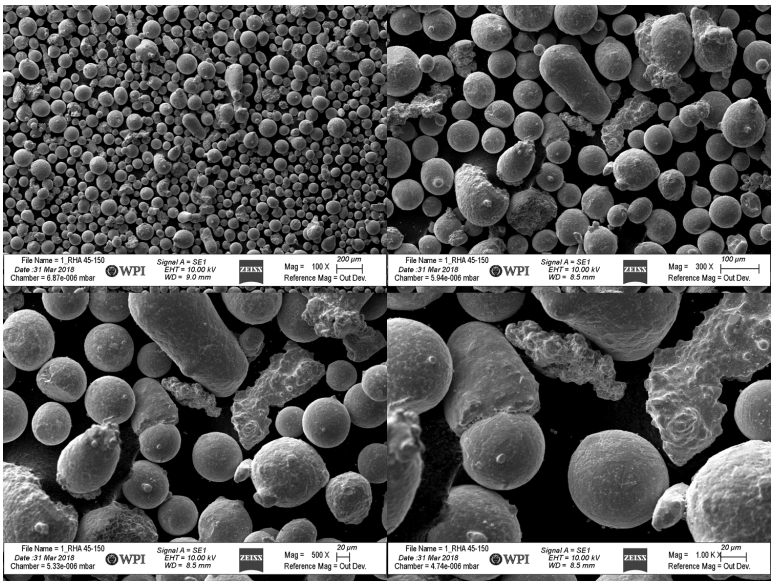

Fig. 13 SEM images of the 45- to 150-µm RHA powder. Scale bars clockwise from top left are 200, 100, 20, and 20 µm.

7.5 Chemical Analysis

Samples of the Al powder and all four powders made from RHA scrap were subjected to chemical analysis by an accredited external laboratory (Luvak Laboratories). The carbon and sulfur were determined through the inert gas fusion technique per ASTM E 1019,[*] while the remainder of the elements were determined using direct current plasma emission spectroscopy per ASTM E 1097.[†] The results are listed in Table 1 for the Al powder and in Table 2 of the RHA powders. The Al powder comprised many elements, as shown in Table 1, but the iron, silicon (Si), magnesium (Mg), copper, and zinc levels were comparable to an Al casting alloy AA355Al. The 0- to 45-µm RHA powder contained a small amount of titanium, which may have been the result of Mobile Foundry contamination. It also appears the carbon and chromium contents were slightly lower in the revert powder, which was gas-atomized with scrap from the first run.

[*] Standard test methods for determination of carbon, sulfur, nitrogen, and oxygen in steel, iron, nickel, and cobalt alloys by various combustion and inert gas fusion techniques. ASTM International; 2018.

[†] Standard guide for determination of various elements by direct current plasma atomic emission spectrometry. ASTM International; 2017.

Table 1 Results of chemical analysis: Al powder (wt%)

Element	Aluminum 0–45 µm
Aluminum	Balance
Oxygen	0.096
Nitrogen	0.001
Carbon	0.015
Sulfur	<0.001
Iron	0.98
Silicon	4.93
Magnesium	0.75
Manganese	0.29
Copper	1.47
Gallium	0.012
Nickel	0.018
Lead	0.037
Tin	0.014
Titanium	0.11
Zinc	0.095

Table 2 Results of chemical analysis: RHA powder (wt%)

Element	RHA 0–45 µm	RHA 45–150 µm	RHA 0–45 µm (Revert)[a]	RHA 45–150 µm (Revert)[a]
Iron	97.8	98.0	98.1	98.1
Nickel	0.029	0.028	0.028	0.027
Chromium	0.32	0.32	0.27	0.27
Manganese	1.05	1.03	1.00	1.02
Carbon	0.167	0.170	0.154	0.151
Molybdenum	0.13	0.11	0.12	0.11
Silicon	0.27	0.26	0.26	0.27
Sulfur	0.005	0.004	0.004	0.005
Phosphorus	0.019	0.018	0.018	0.017
Titanium	0.12	…	…	…

[a]Revert represents a rerun to gas-atomize powder from the scrap of the first run.

8. Additive Manufacturing Using Recycled Metal Powder

Much documentation exists with respect to the reuse of metal powder for AM.[23–27] Of course, this is advantageous because of the material and subsequent financial savings. These articles detail the procedures of powder recovery and characterization, provide cost models, and even estimate the number of times metal powder can be reused. It was difficult to find any documentation of research into melting and gas-atomizing scrap metal into usable AM-grade powder. The powder made from the scrap Al was subjected to cold-spray repair simulations at ARL and AFS repair simulations at MELD. The powder made from scrap RHA was subjected to LPBF additive manufacturing at MolyWorks and ARL.

8.1 Cold Spray of Powder from Scrap Aluminum

Two metal AM techniques have the potential to be used in an expeditionary (portable, mobile) capacity: cold spray and AFS. As long as ancillary requirements such as power, gas supplies, hardware platform, and more exist, these technologies could be used at the point of need in the near future. As a proof-of-concept, the all-scrap Al powder was subjected to cold spray and AFS trials.

The portable VRC Metal Systems Generation-II cold-spray unit located at ARL was used for the cold-spray trials. Substrates with simulated damage (grooves representing blended regions where cracking or corrosion could have occurred in the field) were subjected to the following VRC parameters using helium as the carrier gas:

- Nozzle 9 (2-mm throat × 4-mm exit diameter, 120 mm long)
- Carrier gas flow rate: 159 standard liters per minute
- Temperature: 350 °C; pressure: 450 psi
- Application: hand-sprayed

Cold spray is a powder-consolidation process whereby powder is mixed with a carrier gas and transmitted through a converging/diverging rocket nozzle for deposition onto a substrate (Fig. 14).

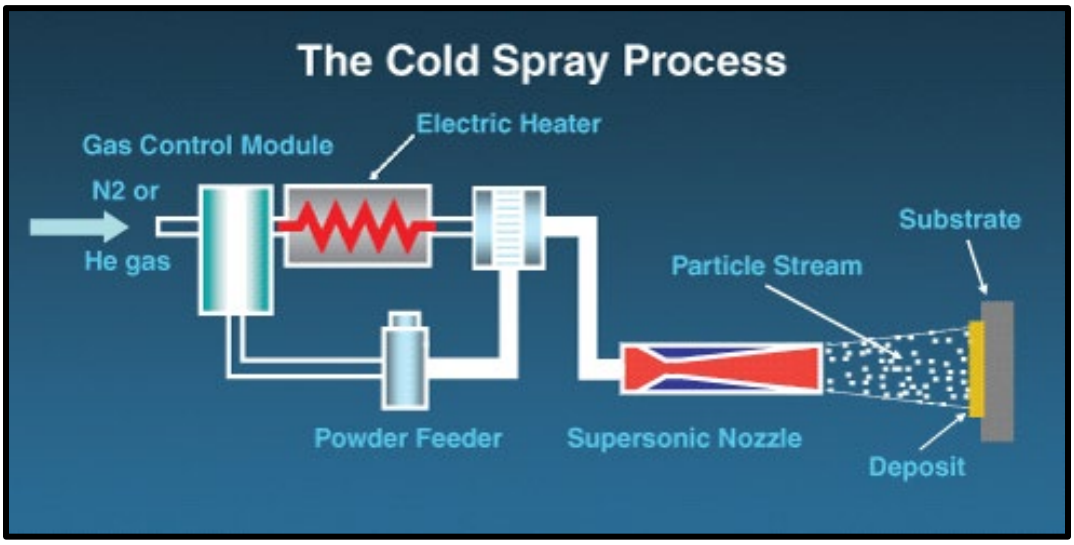

Fig. 14 Cold-spray process

Two of the grooves on each panel were filled with the all-scrap Al powder, and one of the grooves on each panel was milled down to show the fill. Visually, it appeared that this powder could be deposited using cold-spray technology (Fig. 15). Figure 16 shows a magnified view of one of the smaller panels.

Fig. 15 Three Al panels showing cold-spray deposits of all-scrap Al powder with one groove on each panel milled to show fill

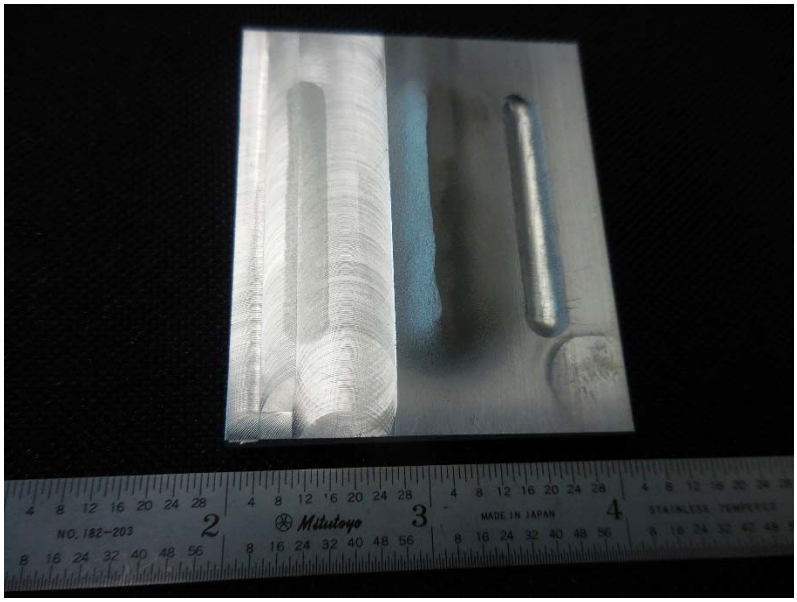

Fig. 16 Magnified view of one of the small panels with milled surface on the left

One of the smaller panels was sectioned and subjected to metallographic examination. Analysis focused on the cold-sprayed groove that was subsequently milled. Figure 17 shows the groove filled with the cold-spray deposit, while Fig. 18 shows a magnified view of the mechanical mixing that occurred between

the cold-spray deposit and the substrate, indicative of a strong adhesive bond in that region. However, in another region (Fig. 19), it was noted that the adhesion was less than ideal, and that future cold-spray depositions should be optimized to account for this lesson learned. Figure 20 shows a magnified view of the mechanical mixing.

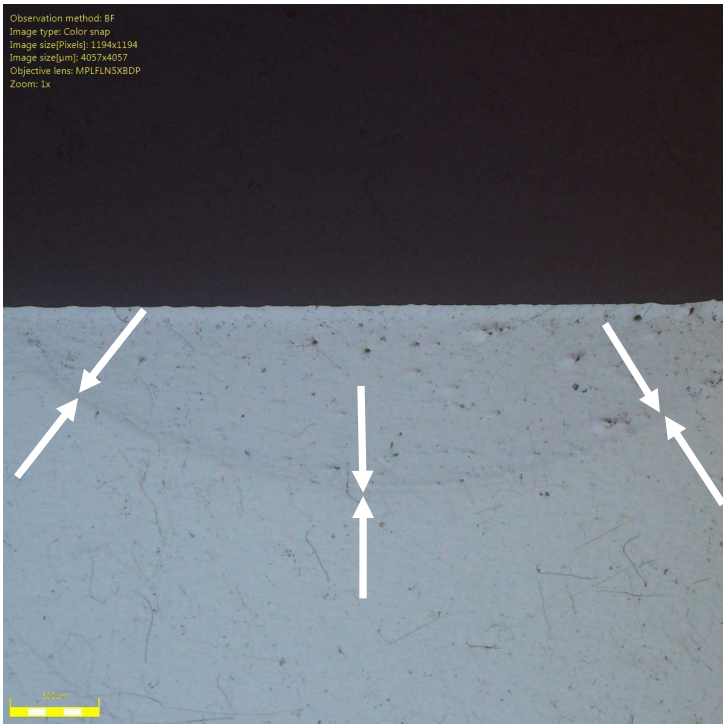

Fig. 17 Metallographic cross section of groove filled with cold-sprayed deposit, and subsequently milled. Arrows delineate interface of deposition and substrate. Scale bar = 500 µm.

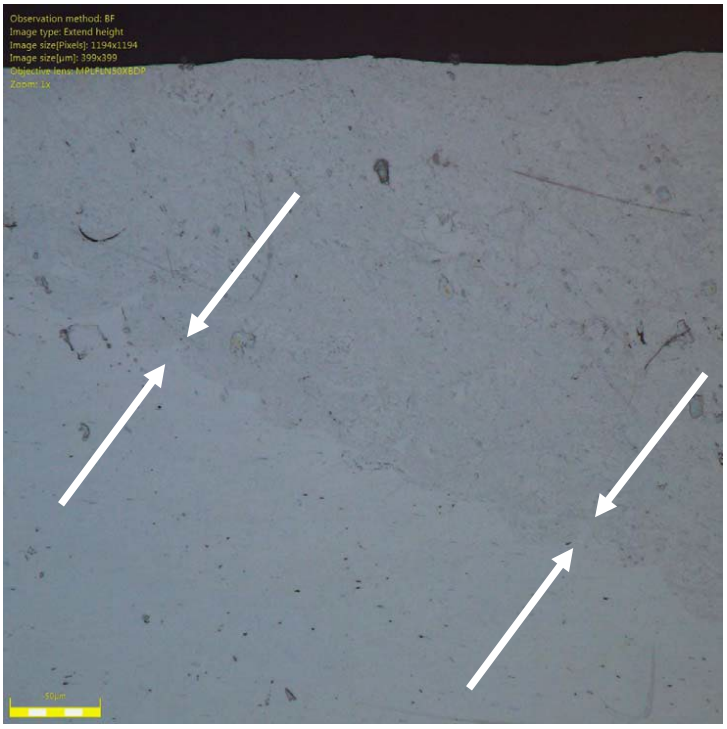

Fig. 18 Magnified view of interface between cold-spray deposit and substrate, showing mechanical mixing. Arrows delineate interface of deposition and substrate. Scale bar = 50 µm.

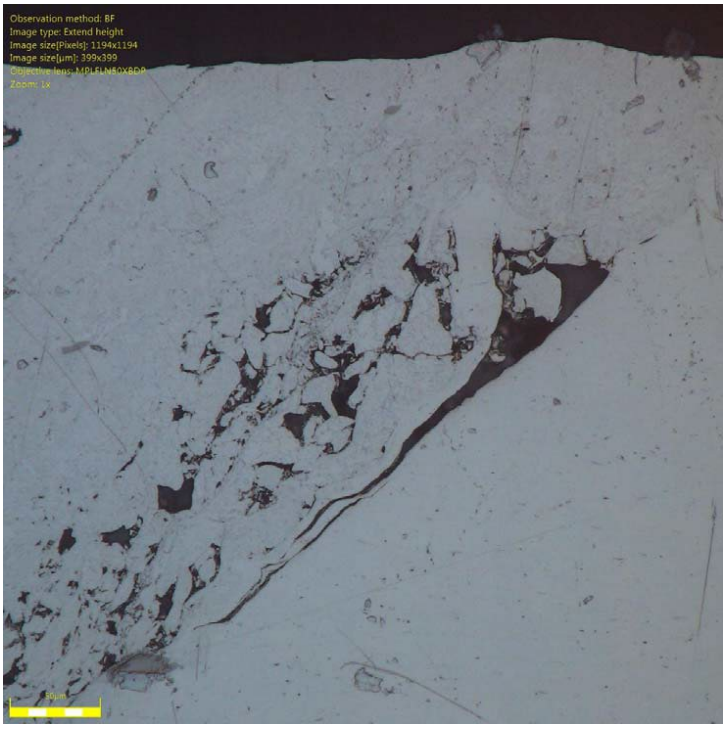

Fig. 19 Region of the interface between cold-spray deposit and substrate where adhesion was less than optimal. Scale bar = 50 µm.

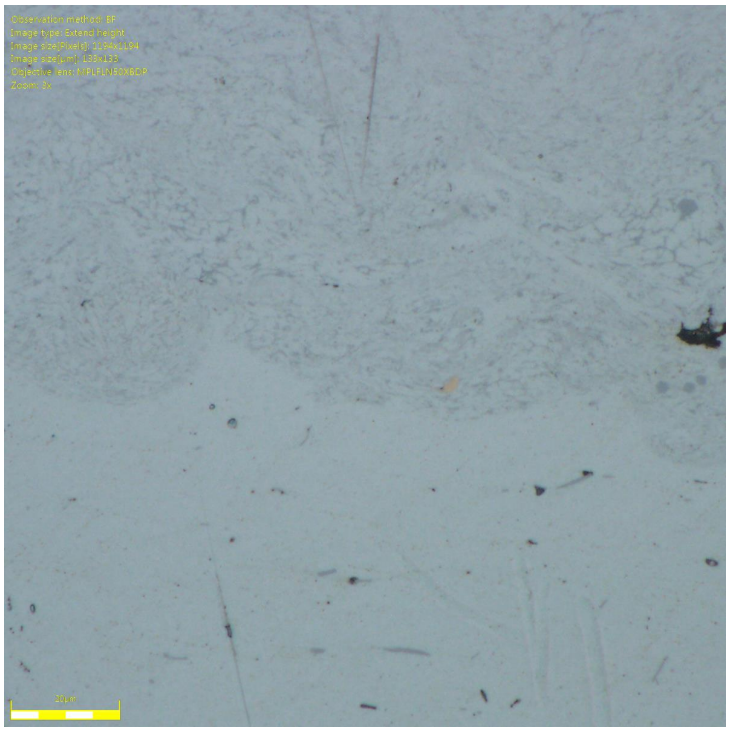

Fig. 20 Magnified view of the mechanical mixing at the interface. Scale bar = 20 µm.

The cold-sprayed panels were subjected to computed tomography (CT) inspection to determine the presence of defects. A NorthStar X5000 X-ray CT system was used to scan the six AFS samples with the scan settings of 220 kV, 450 µA, 2250 projections, and a voxel size of 56 µm. Considering both the base plate and the powder made from the scrap material were both Al alloys, it was surprising to see sufficient contrast between the two materials, as shown in Fig. 21. This indicates that the alloying elements within the different aluminums were sufficient to lead to a difference in the X-ray mass attenuation coefficients. As shown in Fig. 21, there were some areas of incomplete fusion between the deposit and the substrate as represented by the darkened areas. This corroborates the metallography findings.

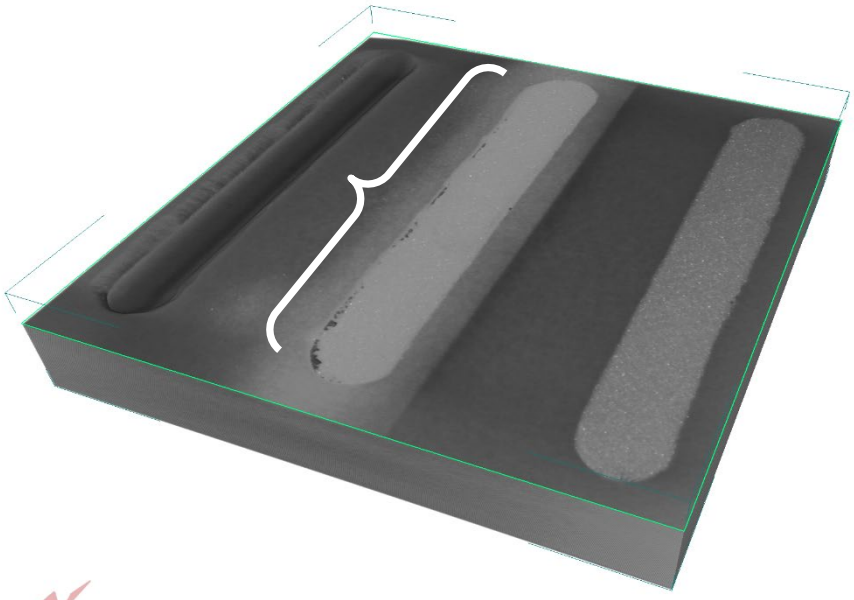

Fig. 21 CT of a representative cold-sprayed panel with bracket showing incomplete adhesion along the edge of the middle section

8.2 Additive Friction Stir Processing of Powder from Scrap Al

Six panels (Fig. 22) with simulated damage were subjected to the patented MELD AFS process using the Al powder made from scrap in the Mobile Foundry. As shown in Fig. 23, this process feeds "filler" material through a hollow tool. The filler material is under force while the hollow tool rotates. A combination of shear and friction plastically deform both the filler material and the material receiving the deposit. In this state, the two can be "stirred" together, creating a fully bonded, fully dense structure. Though Fig. 23 shows a solid metal rod, the equipment can also use powder. AFS is a solid-state process, with no melting of the powder, rod filler, or the substrate. The dynamic recrystallization of the plastically deformed grains leads to low residual stresses. MELD has demonstrated the ability to process a wide range of powder shapes and sizes, and offers a portable machine, as shown in Fig. 24. MELD processed the material in open atmosphere, with no gas, at ambient temperature. Fig. 25 (left) shows a representative Al substrate panel fixtured on the machine. An excess of material was deposited, as shown in Fig. 25 (right). Further efforts refined and minimized the filler material used. The milled-down repaired sample is shown in Fig. 26.

Fig. 22 AA6061 Al panels with simulated damage, and the Al powder (–325 mesh) made in the MolyWorks Mobile Foundry using scrap Al as the feedstock

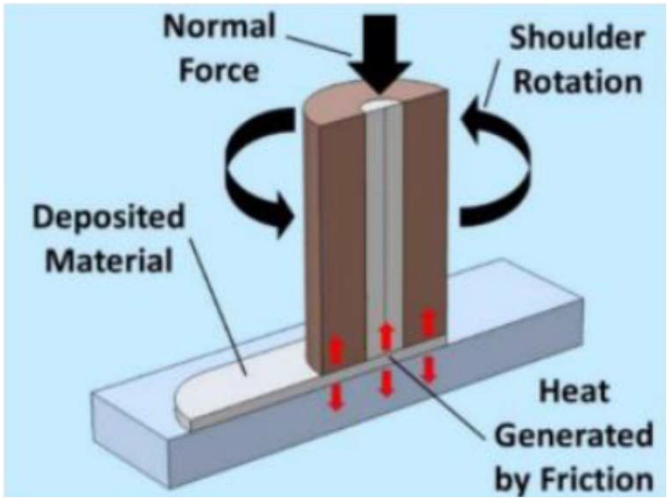

Fig. 23 Schematic illustrating the technology behind AFSP

Fig. 24 MELD B8 model machine and its fit inside an ISO container

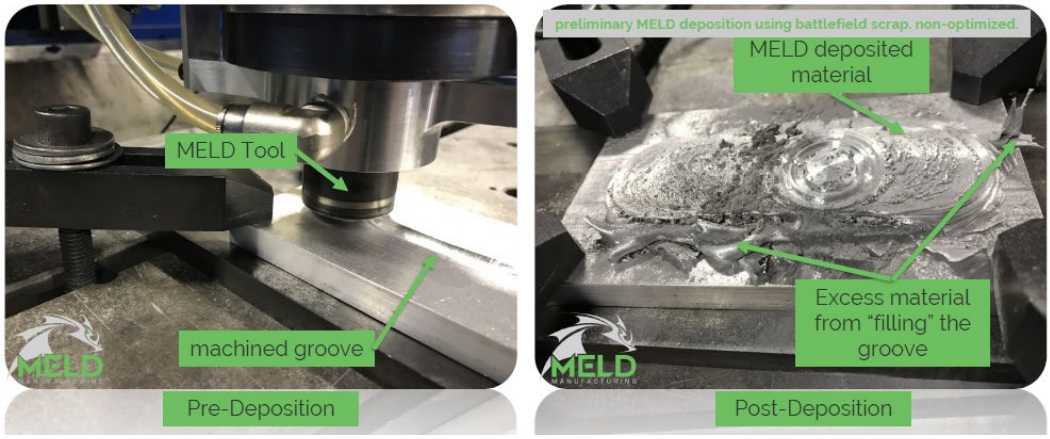

Fig. 25 Representative Al substrate panel: (left) before and (right) after the AFS treatment

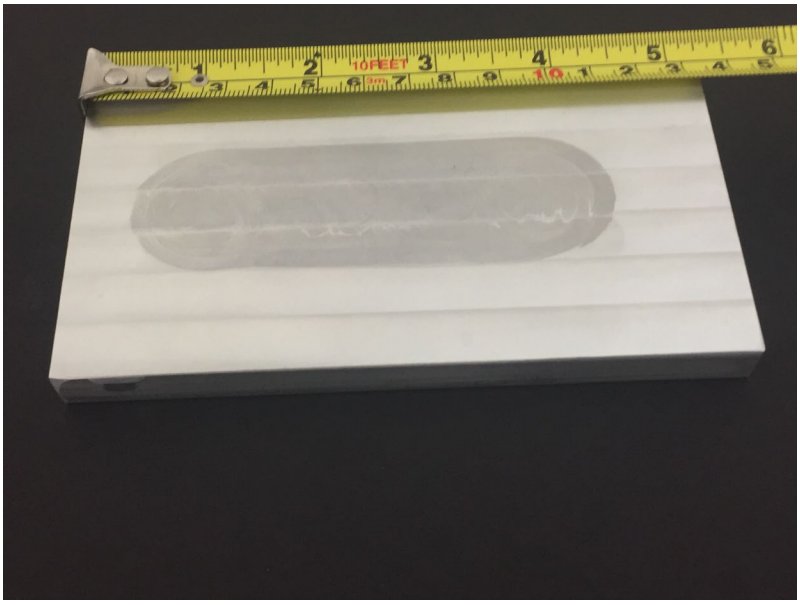

Fig. 26 Panel shown in Fig. 25 (right) after excess Al deposited by AFS was milled down

The panels subjected to AFS were also inspected by CT. The same equipment and settings previously outlined were used for this inspection. As shown in Figs. 27 and 28 (representative inspection from one of the six panels inspected), there was no evidence of defects as a result of the AFS process.

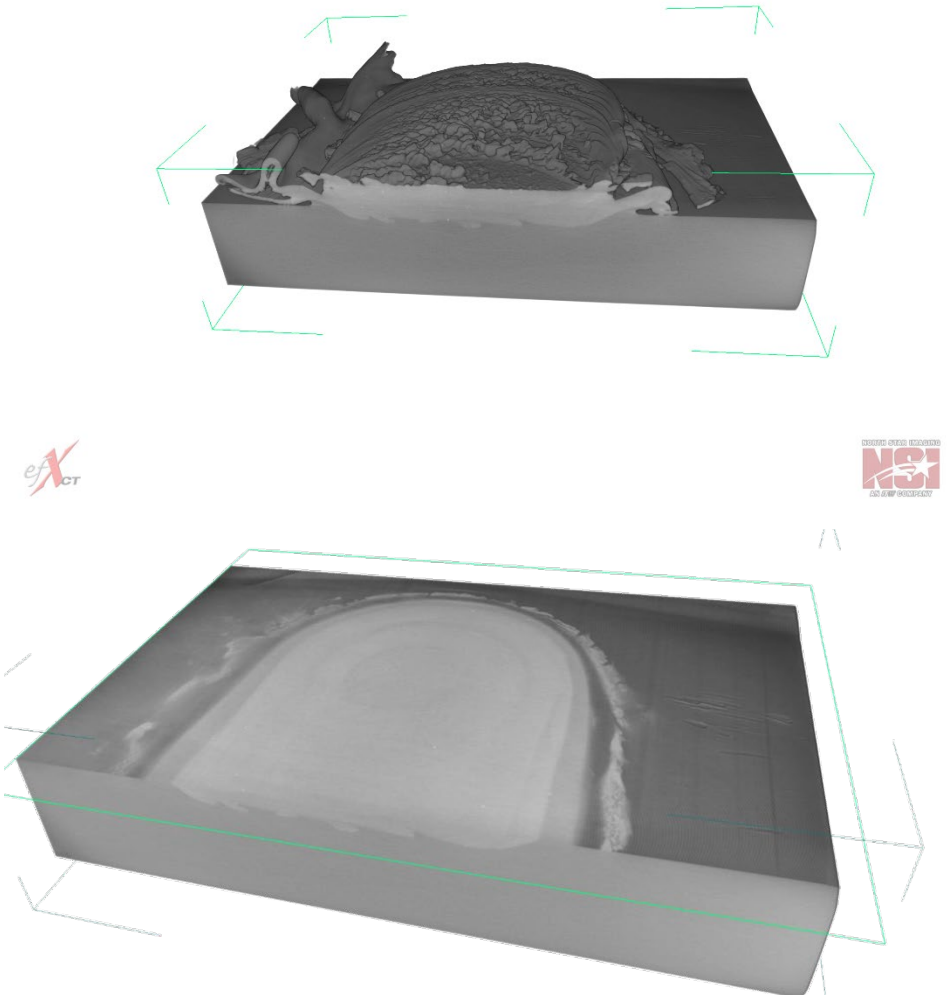

Fig. 27 CT cross section of (top) Sample 1, with (bottom) virtual slice approximately flush with the surface

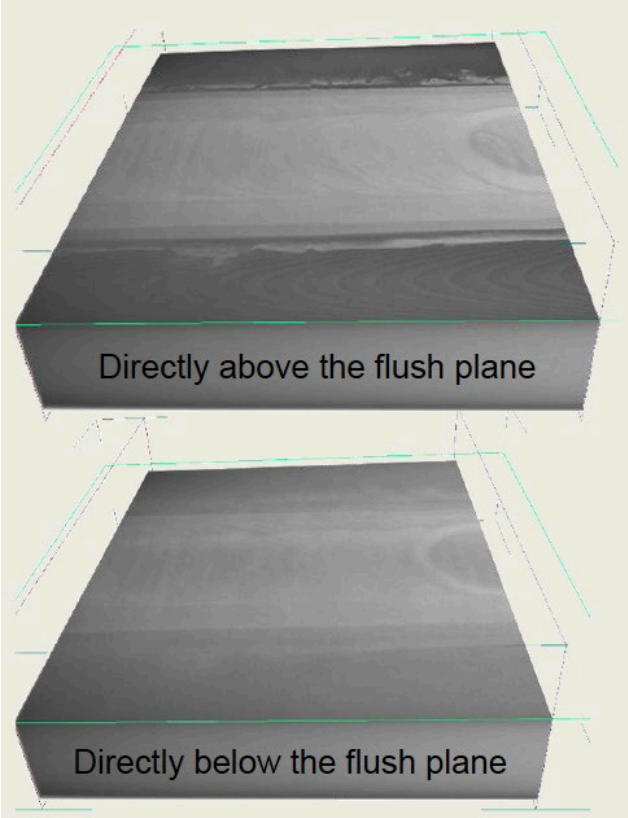

Fig. 28 CT cross section of Sample 1, showing (top) region directly above the flush plane and (bottom) directly below the flush plane

An additional cross section of a panel subjected to AFS was cut and polished using standard metallographic preparation techniques. SEM and EDS were performed on a ThermoFisher Scientific Quanta SEM at the Nanoscale Characterization and Fabrication Laboratory. Electron backscatter diffraction (EBSD) was performed on the FEI Helios 600 Nanolab. As seen in Fig. 29, the microstructure of the deposited material consisted of numerous particles and precipitates distributed in an Al matrix. This is a sharp contrast to normal microstructures for Al–Si alloys, which usually consist of large dendrites of Si or Si–Mg particles. Closer inspection of the material revealed three main types of particles: large and often faceted particles (>1 μm), small oblong particles (~1 μm), and numerous spherical nanoparticles. All but the large particles were too small to get conclusive results from with EDS; however, it still revealed which elements were in higher concentration in the different particles. Figure 30 shows multiple views of the microstructure as well as the summary of the EDS results. From these results, it is likely that the largest particles are iron or steel impurities. These are likely from the recycled nature of the powder, as the iron content in the recycled powder was higher than the standard for AA355. The micron-sized particles are most likely elemental Si or Mg_2Si particles. The morphology of these particles is similar to the broken up Si left in an

A356 Al that was altered via friction stir processing, a process with similar mechanical action to MELD.[28] Lastly, the small copper-rich nanoparticles are likely Al_2Cu precipitates, but transmission electron microscopy would need to be done to confirm this hypothesis. The EBSD results, seen in Fig. 31, show a small average grain size with equiaxed grains. Grain-boundary orientation and resolution were impeded by the large amount of precipitates in the material. Overall, this microstructure is not typical of cast Al–Si alloys, but not necessarily detrimental to their performance. In an friction-stir-processing study of A356 Al, the cast material was transformed into a similar microstructure to the MELD sample. The result was a marginal decrease in the yield strength of the material with a substantial increase to the material's ductility.[28]

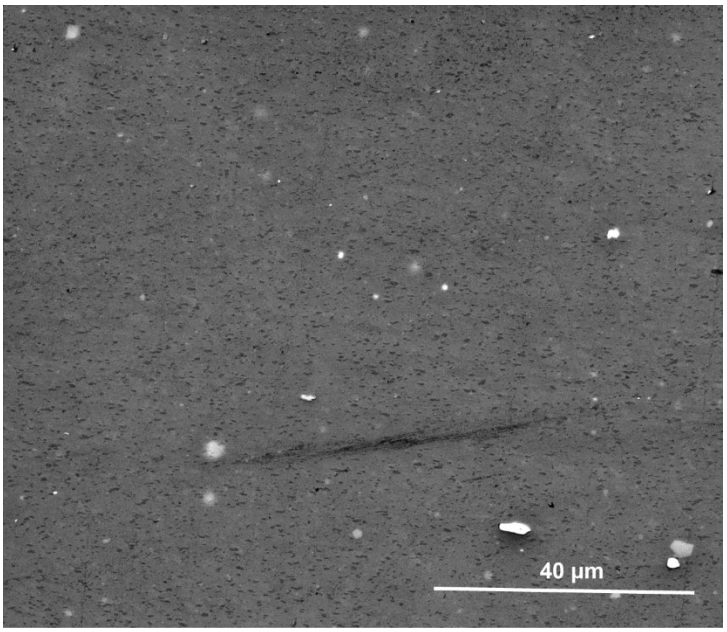

Fig. 29 SEM of AFS fabricated sample cross section

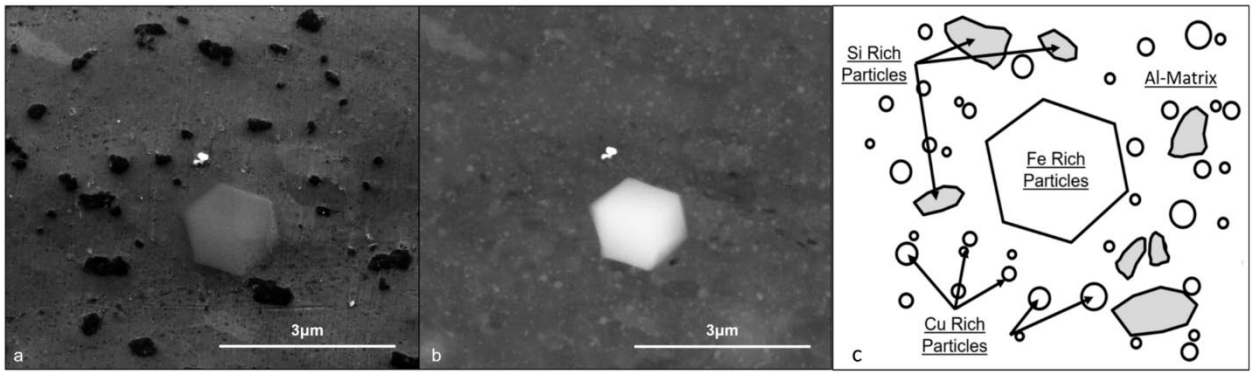

Fig. 30 a) Secondary electron image of microstructure, b) backscattered electron image of microstructure, and c) overview of element concentration results from EDS

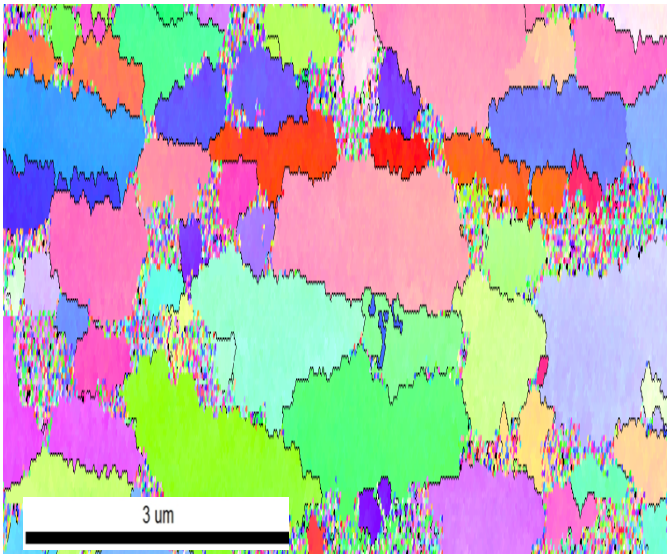

Fig. 31 EBSD map of the Al with significant noise caused by precipitate phases

Vickers microhardness traverses were taken through both the cold-sprayed and AFS depositions. Figures 32 and 33 show figures of the actual readings as well as graphical output of the hardness levels for cold-spray deposition. Figures 34 and 35 show the same for the AFSP sample. It was interesting that a higher gradient existed between the cold-spray deposit/substrate versus the AFSP deposit/substrate, suggesting increased plastic deformation occurred as a result of the cold spray process.

Fig. 32 Vickers microhardness traverse through the cold spray deposit into the substrate. Arrows delineate deposition/substrate interface. Scale bar = 500 µm.

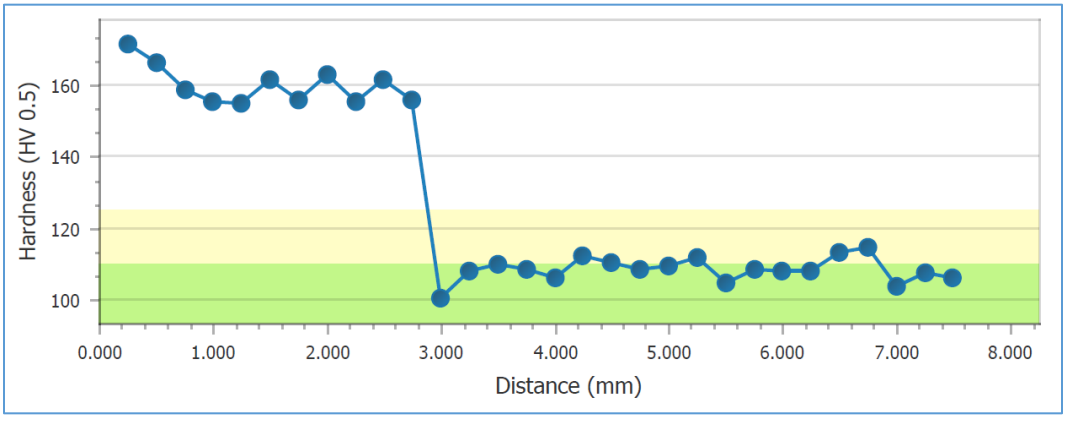

Fig. 33 Representation of the hardness vs. distance from surface for the cold-sprayed sample

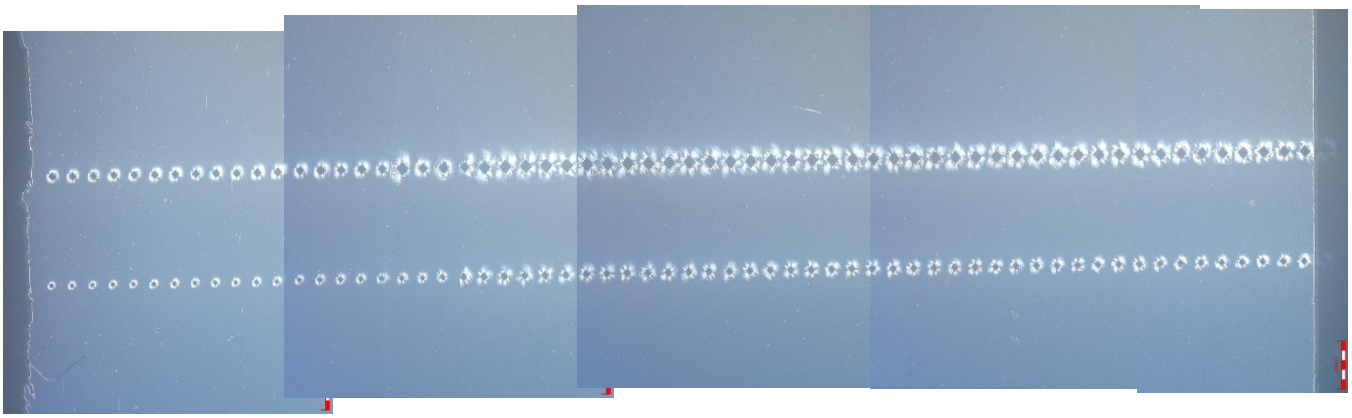

Fig. 34 Vickers microhardness traverse through the AFSP deposit into the substrate. Arrows delineate deposition/substrate interface. Scale bar = 500 µm.

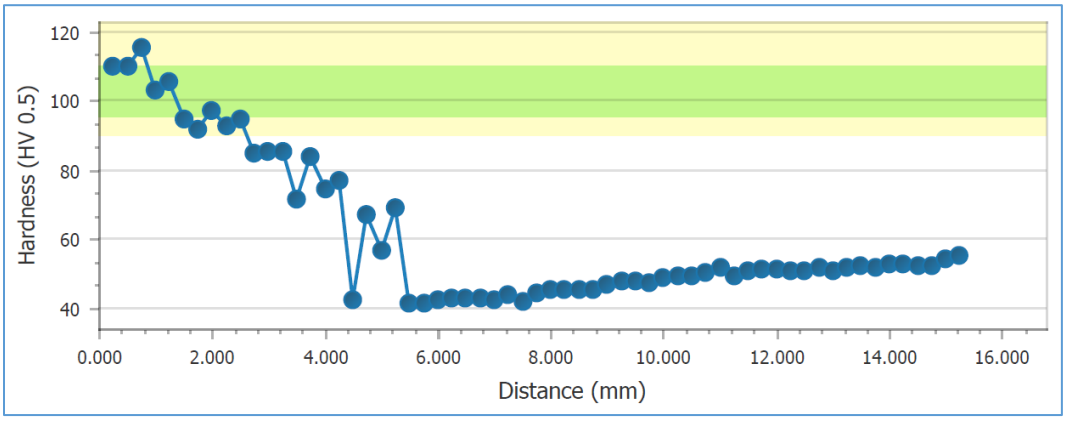

Fig. 35 Representation of the hardness vs. distance from surface for the AFSP sample

8.3 Laser Powder Bed Fusion of Powder from Scrap RHA

MolyWorks showed the powder from scrap RHA could be used to print an object on the EOS M100. A widget was created using their default 316L stainless steel parameters. Knowing that the powder could be used for AM, ARL subsequently printed test specimens on their EOS M100 using varied parameters but settled on what appeared to be optimized parameters similar to those used on a Department of Defense–relevant steel.

Once parameters of the LPBF deposition were optimized, the finalized build was completed (Fig. 36). From this, three tensile specimens were machined and the buttons used for metallography, X-ray CT, and hardness testing.

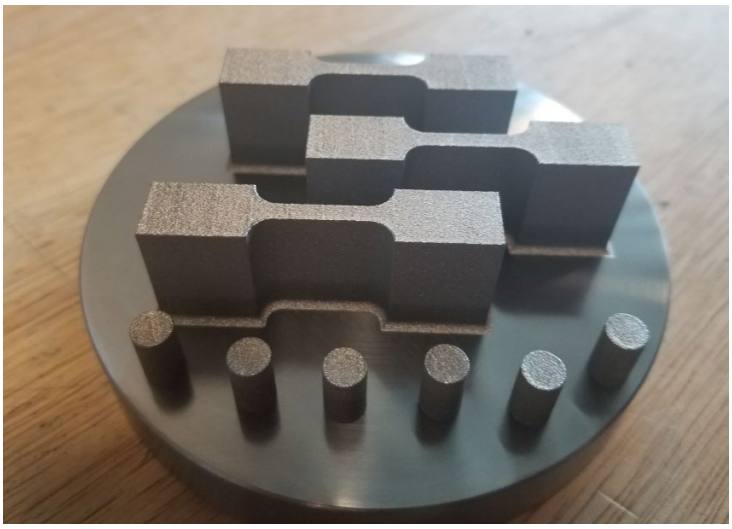

Fig. 36 LPBF AM build plate using scrap RHA powder gas-atomized in an ISO shipping container

The build plate was stress-relieved by loading it into an oven and ramping up to 600 °C for 2 h (followed by air cool) prior to machining the specimens. Buttons were metallographically prepared with a 2% nital etchant and examined. The resultant structure is shown in Fig. 37, left image. The photo on the right is from Konca[29] and shows the tempered martensitic structure of RHA plate in the as-received condition, which compares favorably to the AM-built structure. The refined grain structure of the AM build is likely due to the high heating and cooling rates caused by the AM process. The structure consisted of fine lath martensite, which is consistent with the structure of a carbon steel that has been austenitized, quenched, and tempered. The rapid cooling created during LPBF produces a similar result.

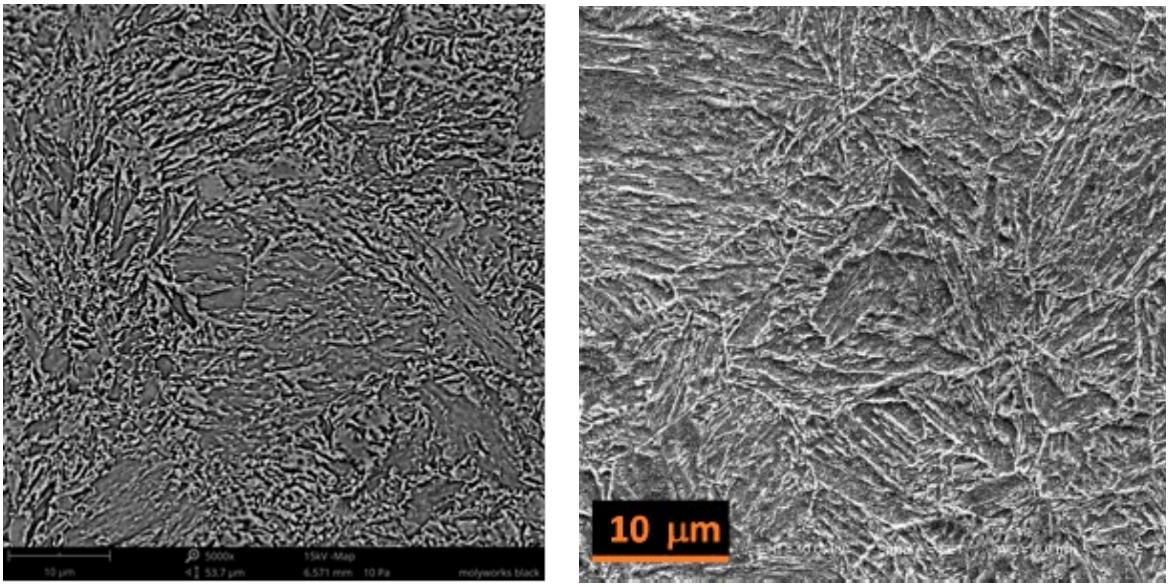

Fig. 37 (left) Representative SEM micrograph of the structure of the LPBF AM build using scrap RHA powder gas-atomized in an ISO shipping container. (right) SEM micrograph of RHA at same magnification for comparison.[29]

The stress-relieved buttons were subjected to Vickers microhardness testing. The readings were taken on a Wilson Micro Hardness tester using a mapping technique taken at 1- × 1-mm intervals, and the results of 45 readings showed that the material averaged a value of 436 ± 12 Vickers-scale hardness (HV). This result is actually slightly higher than the average of 423 HV typical of RHA in the wrought condition. This is likely due to the refined grain structure caused by the rapid heating and cooling of the manufacturing process,[30] making it comparable to traditionally manufactured RHA without postprocessing.

Cylindrical samples were examined for defects via an X-ray micro-CT with a Zeiss Xradia 5200. The porosity was measured using CTan (Bruker) software, and the visualization of the defects was generated via CTvox (Bruker) software. The visual representation of the defects (Fig. 38) show that they were randomly distributed in the AM part and are generally round in morphology. The AM samples were found to have a density of 99.96%.

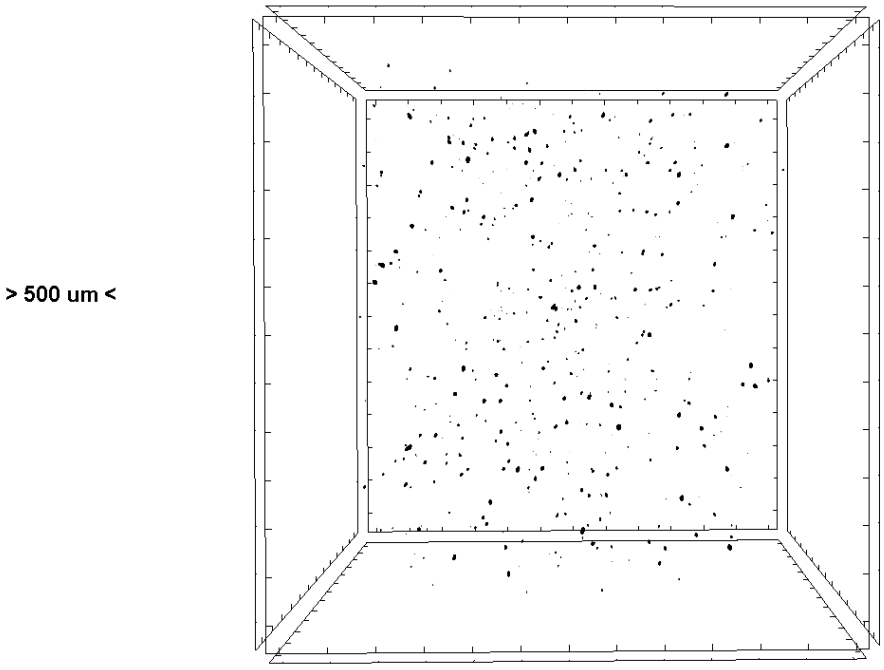

Fig. 38 Porosity mapping of a representative section of the LPBF AM build

Three of the nine aforementioned tensile specimens were subjected to testing using the Instron 5985 Series Universal Testing System. These three were chosen based on optimized build parameters. The average of the three specimens are listed in Table 3, including the yield strength, ultimate tensile strength (UTS), and percent elongation. The mechanical test results listed in Fig. 39 show that the samples were repeatable with very similar stress–strain curves. The variation of elongation is likely a result of local defects in each sample.[31] Although the UTS of the LPBF-built specimens was lower than that of traditional RHA, the yield strength and percent elongation were comparable. The ultimate tensile strength could likely be improved with a post-processing heat treatment.

Table 3 Tensile test results

Material	Yield strength (MPa)	UTS (MPa)	Elongation (%)
AM RHA as stress-relieved	1280 ± 25	1320 ± 4	13 ± 2
Traditional RHA [32]	1200	1700	12

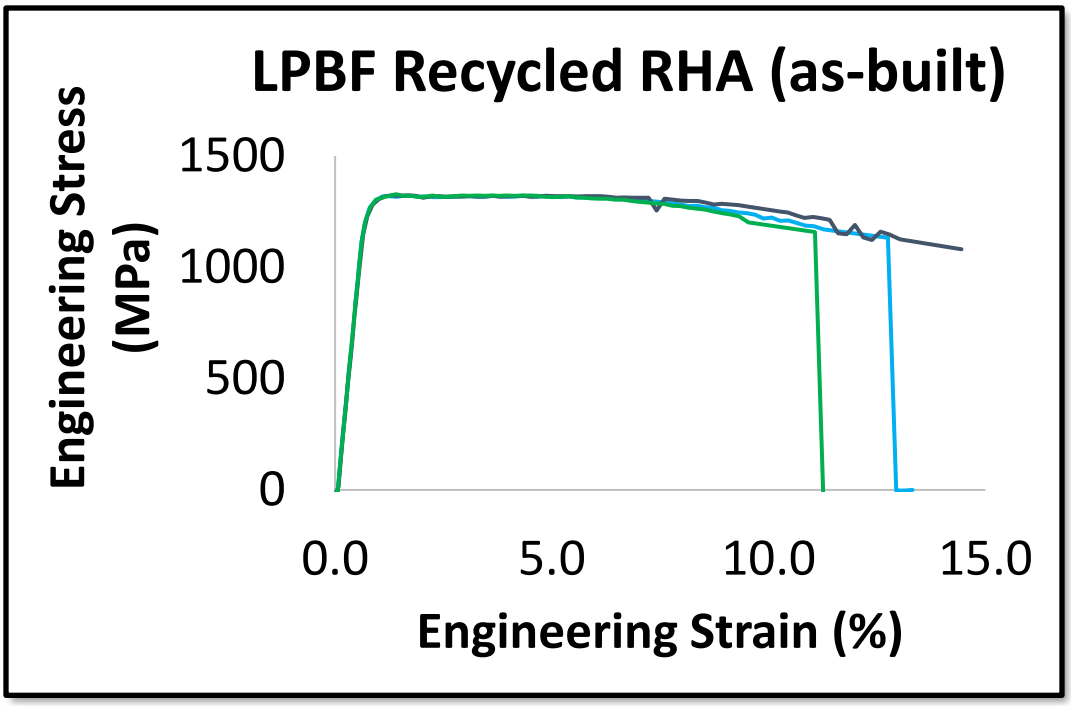

Fig. 39 Results of tensile testing of specimens built via LPBF AM using scrap RHA powder

The monolithic plates shown in Fig. 40 were used for ballistic testing. Testing was conducted on a gas-gun setup described by Yu et al.[33] in accordance with MIL-STD-662F.[34] V_{50} testing was completed using 0.22-cal. fragment-simulating projectile (FSP) rounds at 0° obliquity, and the results were compared with traditional RHA. Targets were impacted by FSPs launched from a smoothbore gas gun. The target stand was located 0.5 m from the gun muzzle. The speed of the projectiles was tracked using a Doppler radar (BR-3502, Infinition Inc.) from the muzzle up to the point of impact. The shot locations on each target were carefully spaced to ensure that the ballistic performance of the target from one impact was not affected by the damage caused by the neighboring impacts. A 0.02-inch-thick Al foil was used as the test witness, which was placed 6 inches behind the target. Any perforation on the witness, by the FSP, or any debris from the target was recorded as complete penetration, whereas no perforation was recorded as partial penetration. The V_{50} value was calculated by the average impact speeds of three of the highest partial penetration and the three of the lowest complete penetration impact speeds. At least 10 shots were taken for each type of targets. The ballistic properties of plates fabricated via LPBF from recycled RHA powder compared very favorably to the results typical of traditional wrought RHA steel, as shown in the following (in fact, they showed a 14% increase):

- V_{50} (0.22-cal. FSP): 440 m/s
- V_{50} wrought RHA (0.22 cal. FSP): 385 m/s

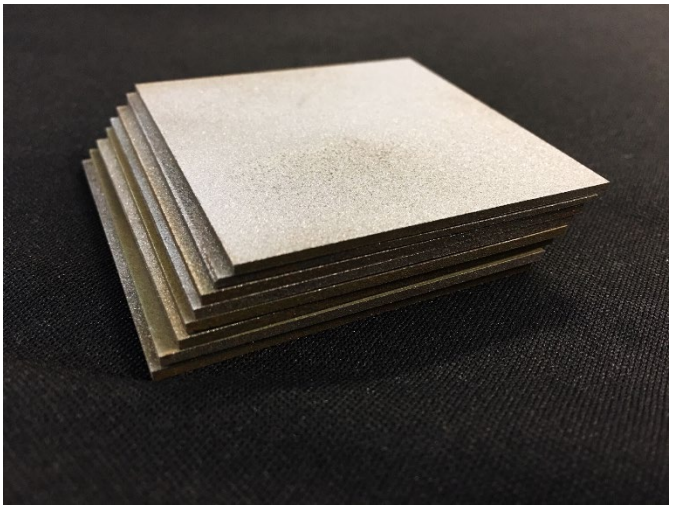

Fig. 40 Ballistic plates built via LPBF AM using scrap RHA powder

9. Conclusions and Lessons Learned

- Scrap Al and scrap RHA was successfully gas-atomized into AM-grade powder in a mobile foundry contained within an ISO shipping container.
- The 0- to 45-µm Al powder was effectively additively manufactured using cold spray and AFSP.
- The 0- to 45-µm RHA powder was effectively additively manufactured using the LPBF method.
- The resultant structure of the LPBF RHA parts was martensitic, exhibiting high strength.
- AM-built plates made from the powder from scrap RHA achieved a 14% increase in ballistic performance against 0.22-cal. FSP compared with wrought RHA.
- The first-ever LPBF processing parameters for RHA were developed.

10. Recommendations

- Much of the work described herein is cursory in nature, intended as an "art of the possible" to show proof-of-concepts of what may be possible on tomorrow's battlefield. Future work could include a design of experiments to more fully allow exploitation of these technologies to truly lead to transformational overmatch.
- Although this work showed promising results, more effort should be focused on the actual science to better understand the metallurgy behind these successes.

11. References

1. Secretary of the Army. US Army directive 2019-29. Enabling readiness and modernization through advanced manufacturing. 2019 Sep 18. https://armypubs.army.mil/epubs/DR_pubs/DR_a/pdf/web/ARN19451_AD2019-29_Web_Final.pdf.
2. Ransom DS. Logistics transformation – reducing the logistics footprint. US Army War College; 2002 Apr 5.
3. da Silva J, Rezende R. Additive manufacturing and its future impact in logistics. Proceedings of the 6th IFAC Conference on Management and Control of Production and Logistics, 2013 Sep 11–13; Fortaleza, Brazil. Elsevier; c2013.
4. Manners-Bell J, Lyon K. The implications of 3D printing for the global logistics industry. Transport Intelligence. 2012 Aug.
5. Dellarocco GJ. Force projection research and development: the key enabler for Army transformation. US Army War College; 2001 Apr 10.
6. Samarjy R, Kaplan A. Using laser cutting as a source of molten droplets for additive manufacturing: a new recycling technique. Materials & Design. 2017 July 5;125:76–84.
7. Fullenwider B, Kiani P, Schoenung, JM, Ma K. Two-stage ball milling of recycled machining chips to create an alternative feedstock powder for metal additive manufacturing. Powder Technology. 2019;342:562–571.
8. Pepi M, Hardwick N, Sietins J, Cox C, Griffiths J, Yu H, Eonta C, LaTour A, Charles M, Cote D, Sun J. Progress towards expeditionary production of AM-grade metallic powder and subsequent additive manufacturing applications. Presented at the RAPID Conference; 2019 May 20; Detroit, MI.
9. Jordon J, Allison PG, Phillips BJ, Avery DZ, Kinser RP, Brewer LN, Cox C, Doherty K. Direct recycling of machine chips through a novel solid-state additive manufacturing process. Materials and Design Journal. 2020;193:108850.
10. Mahmood K, Khan A, Pinkerton A. Laser metal deposition of steel components using machining waste as build material. Proceedings of the Optical Society of America CLEO Applications and Technology Conference; 2011 May 1–6; Baltimore, MD. ISBN: 978-1-55752-910-7.

11. Jackson MA, Kim A, Mander JA, Thoma DJ, Pfefferkorn FE Production of mechanically-generated 316L stainless steel feedstock and its performance in directed energy deposition processing as compared to gas-atomized powder. CIRP Journal of Manufacturing Science and Technology. 2020;31:233–243.
12. Keck B, Graedel T. Challenges in metal recycling. Science. 2012 Aug;337.
13. Birat J-P. Life-cycle assessment, resource efficiency and recycling. Metall Res Techno. 2015;112(2):206.
14. Bowyer J, Bratkovich S, Ferhholz K, Frank M, Groot H, Howe J, Pepke E. Understanding steel recovery and recycling rates and limitations to recycling. Dovetail Partners. 2015 Mar 23.
15. Brimacombe L, Ckoleman N, Honess Colin. Recycling, reuse, and the sustainability of steel. Millennium Steel; 2005.
16. Broadbent C. Steel's recyclability: demonstrating the benefits of recycling steel to achieve a circular economy. Springer International Journal of Life Cycle Assessment. 2016;21:1658–1665.
17. Daehn K, Serrenho AC, Allwood JM. How will copper contamination constrain future global steel recycling? Environmental Science and Technology. 2017;51(11):6599–6606.
18. Ohno H, Matsubae K, Nakajima K, Nakamura S, Nagasaka T. Unintentional flow of alloying elements in steel during recycling of end-of-life vehicles. Journal of Industrial Ecology. 2014 Jan 25. doi: 10.1111/jiec.12095.
19. Marique C. Scrap recycling and production of high quality steel grades in Europe. LA Revue de Métallurgie. 1996 Nov.
20. Whittington WR, Turnage S, Oppedal AL, Hammi Y. Capturing the effect of temperature, strain rate, and stress rate on the plasticity and fracture of rolled homogeneous armor (RHA) steel. Materials Science & Engineering A. 2014;594:82–88.
21. Prifti J, Castro M, Squillacioti R, Cellitti R. Improved rolled homogeneous armor (IHRA) steel through higher hardness. Army Research Laboratory (US); 1997 Apr. Report No.: ARL-TR-1347.
22. Sousa B, Tsaknopoulos D, Massar C, Cote D, Fitzpatrick-Schmidt K, Wlade C, Gleason M, Grubbs J. Characterization of metallic gas atomized powders made from recycled battlefield scrap. Worcester Polytechnic Institute; 2018 Aug 24.
23. Sarton B, Pond T, Griffith B, Everhart W, Elder L, Wenski E, Cook C, Wieliczka D, King W, Rubenchik A, et al. 316L powder reuse for metal

additive manufacturing. Proceedings of the 28th Annual International Solid Freeform Fabrication Symposium; 2017 Aug 7–9; Austin, TX.

24. Tang HP, Qian M, Liu N, Zhang XZ, Yang G, Wang J. Effect of powder reuse times on additive manufacturing of Ti-6Al-4V by selective electron beam melting. JOM. 2015;67(3):555–563.

25. Barclift M, Joshi S, Simson T, Dickman C. Cost modeling and depreciation for reused powder feedstocks in powder bed fusion additive manufacturing. Proceedings of the 27th Annual International Solid Freeform Fabrication Symposium; 2016 Aug 8–10; Austin, TX.

26. Renderos M, Girot F, Lamikiz A, Torregaray A, Saintier N. Ni based powder reconditioning and reuse for LMD process. Physics Procedia. 2016;83:769–777.

27. Ford S, Despeisse M. Additive manufacturing and sustainability: an exploratory study of the advantages and challenges. Journal of Cleaner Production. 2016;137:1573–1587.

28. Santella ML, Engstrom T, Storjohann D, Pan T-Y. Effects of friction stir processing on mechanical properties of the cast Al alloys A319 and A356, Scripta Materialia. 2005;53(2):201–206.

29. Konca E. A comparison of the ballistic performances of various microstructures in MIL-A-12560 Armor Steel. Metals. 2020 Mar;10(4):446.

30. Nath SD. Irrinki H, Gupta G, Kearns M. Microstructure-property relationships of 420 stainless steel fabricated by laser-powder bed fusion. Powder Technology. 2019;343:738–746.

31. Voisin T, Calta NP, Khairallah SA, Forien J-B, Balough L, Cunningham RW, Rollett AD, Wang YM. Defects-dictated tensile properties of selective laser melted Ti-6Al-4V. Materials & Design. 2018;158:113–126.

32. Jamil WNM, Sajuri Z, Aripin MA, Abdullah S. Mechanical properties and microstructures of steel panels for laminated composites in armoured vehicles. International Journal of Automotive and Mechanical Engineering (IJAME). 2016 Dec;13(3):3742–3753.

33. Yu J, Dehmer PG, Sands JM. The current capabilities on dynamic impact testing. Army Research Laboratory (US); 2008 July. Report No.: ARL-TR-4496.

34. MIL-STD-662F. V_{50} ballistic test for armor. Naval Publications and Form Center; 1997 Dec 18.

List of Symbols, Abbreviations, and Acronyms

AFS	additive friction stir
AFSP	additive friction stir processing
AISI	American Iron and Steel Institute
Al	aluminum
AM	additive manufacturing
APG	Aberdeen Proving Ground
ARL	Army Research Laboratory
CNC	computer numerical control
CT	computed tomography
DEVCOM	US Army Combat Capabilities Development Command
EDS	energy dispersive spectroscopy
EBSD	electron backscatter diffraction
FSP	fragment-simulating projectile
FY	fiscal year
HV	hardness, Vickers scale
ISO	International Organization for Standardization
LENS	laser-engineered net shape
LPBF	laser powder bed fusion
Mg	magnesium
NGIC	National Ground Intelligence Center
OFE	oxygen-free electronic
RHA	rolled homogeneous armor
SBIR	Small Business Innovative Research
SEM	scanning electron microscopy
Si	silicon
UTS	ultimate tensile strength

WPI	Worcester Polytechnic Institute

1 (PDF) DEFENSE TECHNICAL INFORMATION CTR DTIC OCA

1 (PDF) DEVCOM ARL
FCDD RLD DCI
TECH LIB

68 (PDF) DEVCOM ARL
FCDD RLC
C BEDELL
B SADLER
FCDD RLC CA
L KAPLAN
FCDD RLC ES
G VIDEEN
S HILL
Y PAN
FCDD RLC I
S RUSSELL
FCDD RLC N
BM RIVERA
A SWAMI
FCDD RLD
P BAKER
A KOTT
M LAFIANDRA
JC RIDDICK
FCDD RLD D
T ROSENBERGER
FCDD RLD E
KS FOSTER
FCDD RLD F
K KAPPRA
FCDD RLD M
T RYAN
FCDD RLD SM
L BLUM
FCDD RLH
J CHEN
PJ FRANASZCZUK
C LANE
FCDD RLH B
JJ SUMNER
FCDD RLH F
JR GASTON
FCDD RLL
T KINES
FCDD RLL DP
J MCCLURE
FCDD RLR
B HALPERN
S LEE
B WEST
FCDD RLR E
RA MANTZ
C VARANASI
FCDD RLR EL
JX QIU
MD ULRICH
FCDD RLR EN
RA ANTHENIEN, JR
M MUNSON
FCDD RLR IC
MA FIELDS
SP IYER
FCDD RLR IN
XN WANG
FCDD RLR P
P REYNOLDS
FCDD RLR PL
MK STRAND
LL TROYER
FCDD RLS
J ALEXANDER
M GOVONI
M WRABACK
FCDD RLS C
JB CARROLL
FCDD RLS CE
R JOW
K XU
FCDD RLS CL
M DUBINSKIY
FCDD RLS E
RD DELROSARIO
FCDD RLS ED
K JONES
FCDD RLS EA
A ZAGHLOUL
FCDD RLS S
WL BENARD
FCDD RLW
S KARNA
JF NEWILL
AM RAWLETT
SE SCHOENFELD
J ZABINSKI
FCDD RLW B
R BECKER
FCDD RLW D
B MCWILLIAMS
FCDD RLW M
ES CHIN
FCDD RLW MD
M PEPI
A KUDZAL
FCDD RLW MG
J ANDZELM
FCDD RLW S
AL WEST
FCDD RLW T

RZ FRANCART
FCDD RLW TC
JD CLAYTON
FCDD RLW W
TV SHEPPARD
FCDD RLW WA
B RICE
R PESCE-RODRIGUEZ